Energy Reports 7 (2021) 5909–5921

Contents lists available at ScienceDirect

Energy Reports

journal homepage: www.elsevier.com/locate/egyr

Research paper

Parametric analysis and system optimization of a novel steam production system by synthetic cascade utilization of industrial waste heat

Zhiyong Zeng [a], Yufeng Chen [a], Chenghao Li [b], Yunfeng Li [a], Xiaozan Wu [a,*]

[a] School of Energy Science and Engineering, Central South University, Changsha, Hunan, 410083, China
[b] School of Engineering, University of Warwick, Coventry CV4 7AL, UK

ARTICLE INFO

Article history:
Received 24 June 2021
Received in revised form 19 August 2021
Accepted 25 August 2021
Available online 17 September 2021

Keywords:
Waste heat recovery
Steam production
Parametric analysis
System optimization

ABSTRACT

A great deal of waste heat is released in many industrial procedures, resulting in not only serious energy waste but also heat pollution. To alleviate this phenomenon, in-depth analyses of a steam generation system, whose novelty lies in synthesis of mechanical vapor recompression and thermal power conversion processes for dealing with low-grade waste heat utilization, are performed. Determination of organic Rankine cycle (ORC) working fluid and thermal power conversion cycle are conducted in detail. Then, parameter analyses and optimization are investigated. The simulation results show that the ORC–based system performs well in efficiency improvement and cost reduction with 69.41% higher exergy efficiency and 9.66% lower cost per ton of steam than the transcritical carbon dioxide-based system. In addition, there is an optimum flow rate of ORC working fluid for thermodynamic performance. A lower steam compression ratio and a higher heat source temperature are beneficial to improve techno-economic performance. At last, according to optimized results, the steam production yield and exergy efficiency of the ORC–based system are 2.50% and 44.31% under the 100 °C heat source condition, as well as the cost per ton of recycled steam is 7.67 $/ton. The optimizations of the system, working fluid, and parameters provide valuable information for improving system performance.

1. Introduction

1.1. Motivation and problem statement

Extensive attention for energy costs, climate change, as well as environmental pollution demand for the energy efficiency increase and pollution emissions reduction in industrial sector, where the most energy-consuming has been consumed in China, accounting for 68.04% (Fig. 1a) in 2017 (National Bureau of Statistics, 2017). In the industrial procedure, a massive amount of waste heat has been produced, and low-grade waste heat (below 150 °C) accounts for nearly half (Fig. 1b). In typical energy-intensive industries, including cement, steel, and glass, the capacities of low-temperature waste heat potential represent 49%, 66%, and 44% respectively (Lu et al., 2016), as shown in Fig. 1b. Making full use of the above waste heat is conducive to saving fuel, improving production efficiency, and avoiding heat pollution & cooling costs caused by direct emissions. Low-temperature hot water is a common carrier of low-grade waste heat. In many chemical reaction processes, the low-temperature hot water is often around 90–100 °C, and some even higher than 100 °C. For instance, (1) the waste water temperatures of scouring, bleaching, and desizing operations in dyeing process are up to 130 °C, 90∼130 °C and 100 °C (Xu, 2011); (2) The production of phthalic anhydride is accompanied by the discharge of hot water at 120–130 °C (Wang et al., 2019).

Steam is a preferred heat exchange medium in actual production due to its ability to provide stable latent heat. The boiler system is a traditional and the most widely used steam production system. Nevertheless, as part of the clean energy movement, decentralized coal-fired boilers began to be replaced or eliminated by large-scale steam heating systems in Chinese industrial sectors (Wang et al., 2020a). Meanwhile, steam generation by gas-fired and electric boilers is limited by the high production cost. In summary, these conditions heighten the need for the design of energy-efficient, environmentally-friendly (Ammar et al., 2012), and economical (Fitó et al., 2020) systems, which aim at low-temperature waste heat utilization and steam generation.

1.2. Literature review

To improve the efficiency of waste heat utilization, scholars have explored many high-efficiency waste heat recovery technologies, including high-temperature heat pump (HTTP), waste

* Corresponding author.
E-mail address: wuxiaozan@csu.edu.cn (X. Wu).

https://doi.org/10.1016/j.egyr.2021.08.178

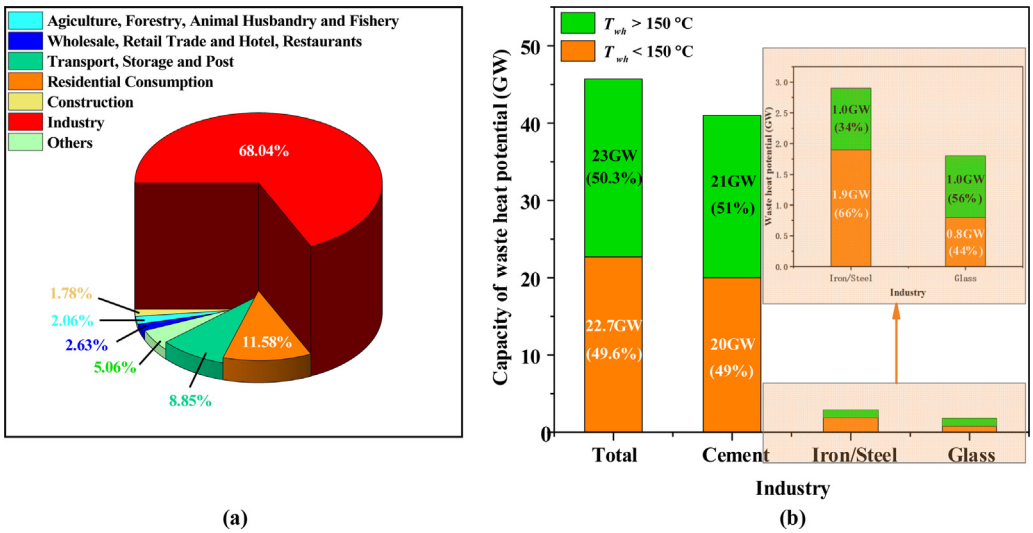

Fig. 1. (a) The proportion of energy consumption in various industries in China. (b) The capacities of waste heat potential in cement, iron, and glass industries.

heat power generation (WHPG), and vapor compression (Iglesias Garcia et al., 2018; Jouhara et al., 2018; Minea, 2014; Wang et al., 2017). In our previous work, the characteristics, advantages, and disadvantages of the waste heat utilization systems were discussed in detail (Chen et al., 2021). The optimizations of these technologies are often conducted in the aspects of thermal power conversion (TPC) technologies, cyclic working fluid, system configuration, and key parameters.

Selecting a proper TPC system is essential to improve cycle performance. It is reported that organic Ranking cycle (ORC), which applies organic substances with low boiling points and high vapor pressures (Quoilin et al., 2013), as working mediums, is effectively applied to low-grade waste heat recovery such as geothermal (Bao et al., 2020; Wang et al., 2020b), biomass (Calli et al., 2021; El-Sattar et al., 2020), and solar (Sinasac and Jianu, 2021) utilization. As important forms of the thermal-power conversion cycle, supercritical CO_2 (S-CO_2) power cycle and transcritical CO_2 (T–CO_2) power cycle have become hot research topics because of their unique characteristics. Liao et al. (2019) thought S-CO_2 power cycle owns the potential for being employed in power generation and combined heat and power generation (CHP) system. The pinch limit of S-CO_2 power cycle is slighter owing to a better temperature glide match. Thus, the thermodynamic performance of that is further improved. Evaporation and condensation pressure of the S-CO_2 cycle are above the critical value, while the condensation pressure of the T–CO_2 cycle at a subcritical state (Sarkar, 2015). For the conversion between the low-grade waste power and power, Sarkar believes that the T–CO_2 cycle performs better in terms of thermodynamics than that of the ORC and S-CO_2 cycle. Nevertheless, the above-mentioned systems operate under extremely high pressure, which puts extremely high demands on the equipment and further increases the costs of the equipment. Consequently, the large equipment investment and operation requirement may become a factor hindering their development.

In addition, the selection of cyclic working fluids is another important means to improve the waste heat utilization efficiency for ORC systems and HTTP systems (Frate et al., 2019; Yu et al., 2016). The selection of working fluids is based on environmental impact, toxicity, system efficiency, and economic feasibility. A new binary, near-azeotropic mixed working fluid called BY-5 was developed by Zhang et al. (2017) for an HTTP system. The coefficient of performance (COP) of the system achieved 2.57 and 4.44 at 80 °C heat source and 130 °C heat sink temperature. Frate et al. (2019) considered that R1233zd(E) is the most appropriate fluid to improve both COP and volumetric heating capacity (VHC) for HTTPs. Saleh et al. (2007) pointed out that the suitable working fluids for three different ORC waste heat utilization systems are ethane, propane, and propylene.

Many recent researches have been devoted to system structure optimization and parameter optimization. A straightforward approach is adding an extra component to improve the thermodynamic efficiency. Kang et al. (2019) and Arpagaus et al. (2018) proposed HTTP systems with an internal heat exchanger (IHX) and a subcooler respectively. Results showed that the former's steam production yield increased by 27 to 31%, and the latter supplied 160 kW heat with less power consumption. What is more, the development of integrated systems is another effective method for waste heat utilization. Sun et al. (2018) compared the system configuration of single-stage ORC, parallel two-stage ORC, and cascade two-stage ORC, and indicated that parallel two-stage ORC is a better selection for lower temperature heat sources. Mateu-Royo et al. (2019) proposed a coupling system based on combined cooling heating and power (CCHP) and ORC for waste heat utilization. The significant performance improvement of 2.44 COP and 8.75% net electric efficiency can be supplied by the coupling system. System coupling significantly improves the overall performance, and it has greater flexibility. At last, optimizing parameters is a common method for system performance improvement. Zhou et al. (2013) and Li et al. (2019a) discussed the effects of heat source temperature, heat source flow rate, superheat degree, and condenser temperature for the ORC–based WHPG system.

1.3. Main contribution

From the above-mentioned literature, it is crucial to make effort on TPC system and working fluid selection, system structure design, and parameter optimization to meet the comprehensive needs of thermodynamics, economy, and energy conservation. In our previous work (Chen et al., 2021), an innovative low-grade waste heat recovery system, which is a coupling of a TPC system and a mechanical vapor recompression (MVR) process, was proposed for the efficient generation of low-pressure steam. The proposed system performs well in waste heat recovery with 37.01% and 60.59% higher exergy efficiencies than two existing reference systems. However, there is still a blank for system optimization and analysis, as well as TPC system and working fluids

selection. For this purpose, a series of efforts are conducted in this study to explore the optimization potential and direction of the proposed system. The results and conclusions of the present study are expected to give a more comprehensive understanding of this novel system in different application scenarios.

The main contributions of this paper are as follows:

(1) The selection of ORC working fluids and TPC subsystems is studied in detail, and selection suggestions based on objectives are given.
(2) The effects of the ORC cyclic fluid flow rate, isentropic and adiabatic efficiency of the expander and pumps, and steam compression ratio (i.e., $P_{steam}/P_{hot\ water}$), on system performance are investigated.
(3) The thermodynamic and economic indicators are calculated after optimization.

2. System description

By the synthetic cascade utilization of the industrial waste heat, the proposed system is dedicated to generating low–pressure steam efficiently and economically. Fig. 2 shows the schematic presentation of the proposed system composed of a TPC subsystem and an MVR subsystem, and Fig. 3 presents the temperature–entropy diagram. The TPC subsystem is composed of five components: an evaporator, a condenser, two pumps (pump 1 and pump 3), and an expander, in which the evaporator also works as the cooler in the MVR subsystem. The MVR subsystem comprises seven parts: two pumps (pump 2 and pump 4), a flash tank, a tee, a heat exchanger, a compressor, and a cooler (it works as the evaporator in the TPC subsystem).

The specific working processes are as follows. Lines of different colors represent streams with various components. The MVR subsystem, utilizing the high-temperature part of the waste hot water (saturated liquid state), is shown on the outside of Fig. 2. Because of the pressure drop, the waste heat is recovered by steam and remaining hot water (processes 1–2 and 1–5). The remaining hot water releases heat in the cooler (process 5–6) and then is separated into two parts, in which one part is discharged to the environment after being pressurized to atmospheric pressure (processes 6–9–18), and the other part is used as the heat sink for the heat exchanger (processes 6–16–7). The purpose of the heat exchanger is to cool the high-temperature steam (state 3). Meanwhile, the steam is compressed by the compressor (process 2–3), and then it released heat (process 3–4). At last, it becomes the target steam. The TPC subsystem is shown on the inside of Fig. 2. Contrary to the MVR subsystem, the TPC subsystem utilizes the waste heat of the relatively low-temperature part. As the heat source of the evaporator, the remaining water heats the cyclic fluid (process 10–11). Then, it flows into the expander for mechanical work generation (process 11–12). After being cooled to the saturated liquid state in the condenser (process 12–15), the fluid is pressurized to a state of high pressure (process 15–10).

We need to pay attention to the coaxial connection between the expander and the compressor in this study, that is, the mechanical power consumption of the compressor is directly provided by the expander. Compared with the conventional configuration, this one avoids the complicated conversion process of work–electricity–work, which is helpful for structure simplification, investment cost reduction, and cycle efficiency improvement. Moreover, the grid provides the mechanical work consumed by pumps 1–4.

3. Mathematical model

3.1. Assumptions

Some specific assumptions are made as follows to simplify the simulation and numerical calculation processes.

- The proposed system operates under steady–state conditions.
- The efficiency of phase separation is set to 100%.
- The heat and pressure losses are ignored in the pipes and heat exchangers.

3.2. Thermodynamic model

3.2.1. Energy and exergy model

The energy and exergy models are built on the basis of the first law and the second law of thermodynamics. The simulation and calculation of the energy transfer between components are by the energy and exergy model.

The exergy model provides a theoretical basis for the calculation of exergy destruction and exergy efficiency. Exergy is defined as the part of energy that can be converted into useful work theoretically under ambient conditions. In general, exergy includes physical exergy, chemical exergy, kinetic exergy, and potential exergy (Liu et al., 2020). In this model, the kinetic and potential exergy is ignorable and chemical exergy is not considered because the combustion is not involved. It takes physical exergy into consideration only, which is defined as:

$$E = m\left[(h - h_0) - T_0\,(s - s_0)\right] \tag{1}$$

where s is the specific entropy, and h is the specific enthalpy.

The energy and exergy correlations for each component are shown in Table S1 in the Supporting Information, and the exergy calculations for the components are shown in Table S2 in the Supporting Information. The subscripts (1,2, …, 18) of balance equations correspond to the status points in Fig. 2.

3.2.2. Thermodynamic index

Analyzing the proposed system, waste heat recovery and low-pressure steam production are the two most important tasks. Hence, steam production yield (η_{sp}), thermal recovery ratio ($\eta_{thermal\,recovery}$), and exergy efficiency (η_E) are three suitable indicators, which can evaluate the performance of the above two tasks in terms of product, energy, and exergy.

The steam production yield shows the productivity clearly. It is closely related to pressure drop in the flash tank, and is calculated as (Lu et al., 2019):

$$\eta_{sp} = (m_4 + m_8)\,/m_1 \times 100\% \tag{2}$$

The thermal recovery ratio is calculated as shown in Eq. (3) given in Box I.

The exergy efficiency is calculated as:

$$\eta_E = \frac{E_{output}}{E_{input}} \times 100\% = 1 - \frac{E_{des}}{E_{input}} \times 100\% \tag{4}$$

where E_{des} is the exergy destruction. The cooling water exergy is too small to be neglected.

The output exergy (E_{output}) is defined as:

$$E_{output} = E_4 + E_8 + W_{exp} - W_{com} - W_{pump\,1} - W_{pump\,2} - W_{pump\,3} - W_{pump\,4} \tag{5}$$

The input exergy (E_{input}) is defined as:

$$E_{input} = E_1 \tag{6}$$

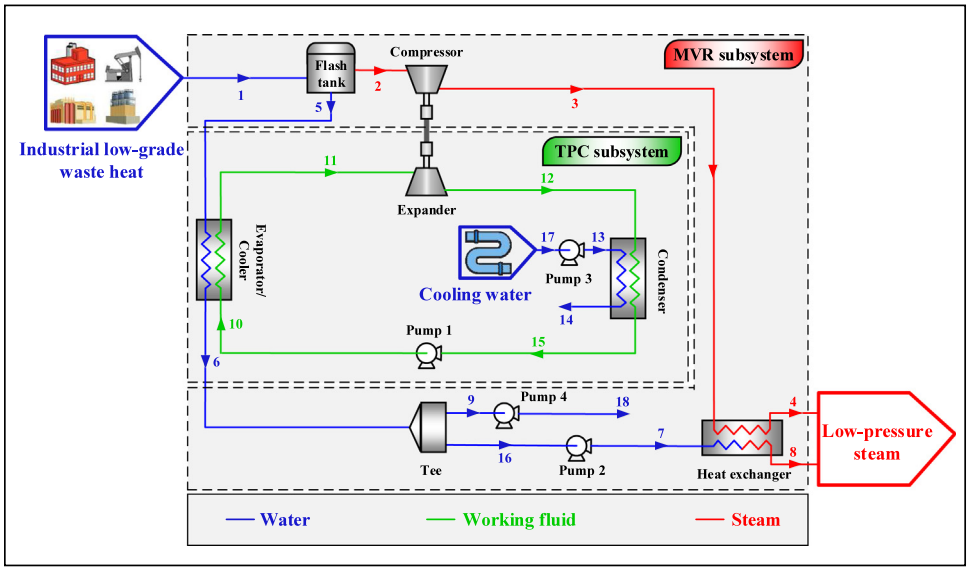

Fig. 2. Scheme of the proposed waste heat utilization system.

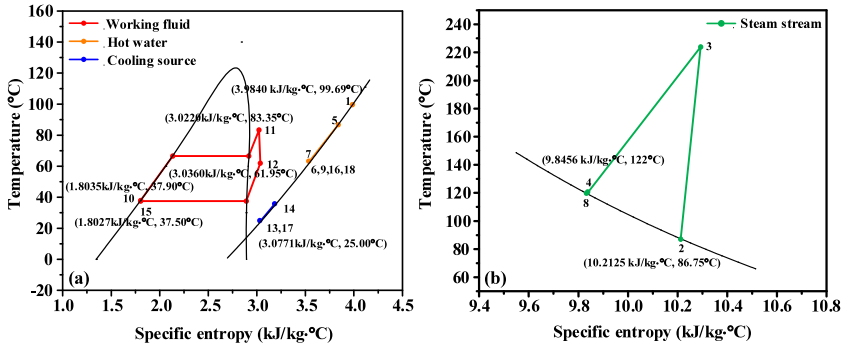

Fig. 3. The temperature–entropy diagram of the proposed system: (a) hot water side and TPC cycle and (b) steam side.

$$\eta_{thermal\,recovery} = \frac{m_4 \cdot (h_4 - h_0) + m_8 \cdot (h_8 - h_0) + W_{exp} - W_{com} - W_{pump1} - W_{pump2} - W_{pump3} - W_{pump4}}{[m_1 \cdot (h_1 - h_0)] \times 100\%} \quad (3)$$

Box I.

3.3. Economic analysis

Economic analysis is a requisite aspect for system performance evaluation owing to its contribution to the feasibility evaluation. For the purpose of generating steam efficiently, cost per ton of recycled (COS) reflects costs of producing unit mass of steam, based on the total costs during the lifetime and the associated steam production (Parrado et al., 2016).

COS is calculated as follows (Chen et al., 2018):

$$COS = \left(CRF \cdot C_{capital} + C_{OM}\right) / M_{steam} \quad (7)$$

where, CRF represents the capital recovery factor, defined as:

$$CRF = \frac{i\,(1+i)^N}{\left[(1+i)^N - 1\right]} \quad (8)$$

where i represents the interest rates, and N denotes the system lifetime.

$C_{capital}$ is the total equipment costs, which is expressed as:

$$C_{capital} = C_{com} + C_{ft} + C_{eva} + C_{exp} + C_{con} + C_{tee} + C_{pumps} + C_{sc} \quad (9)$$

C_{OM} is the operation & maintenance expense, including costs of maintenance (C_{main}), electricity (C_{ele}), and cooling (C_{cool}):

$$C_{OM} = C_{main} + C_{ele} + C_{cool} \quad (10)$$

$$C_{main} = 0.05 \times C_{capital} \quad (11)$$

$$M_{steam} = H \cdot m_{steam} \quad (12)$$

$$H = 0.9 \times 24 \times 365 = 7884 \quad (13)$$

The equipment costs are calculated by the related investment cost functions in the Supporting Information, and detailed information can be found in the original paper (Chen et al., 2021). In this study, the costs of the tee and TPC working media are negligible in comparison with other costs.

3.4. Calculation parameters, optimization processes, and operation strategy

This study applied the powerful engineering simulation software—Aspen Hysys to carry out process simulation. The widely

Table 1
Input parameters for the simulation.

Block	Model	Specification
Flash tank	Separator	• Pressure (state 1): 101.325 kPa • Mass flow rate (state 1): 1.0 kg/s • Vapor fraction (state 1): 0 • Pressure drop: optimization variable
Compressor	Compressor	• Adiabatic efficiency: 85% (Wright, 2013)
Heat exchanger	Heat exchanger	• Outlet pressure (states 4 and 8): 101.325–506.625 kPa (adjustable in Parametric analysis) • Outlet vapor fraction (states 4 and 8): 1
Evaporator/Cooler	Heat exchanger	• Outlet temperature (state 6): optimization variable • Pressure (state 10): adjustable for judging criterion • Mass flow rate (state 10): optimization variable • Overall heat transfer coefficient: 850 W/(m^2 K) (Li et al., 2019b)
Expander	Expander	• Adiabatic Efficiency: 60%–95% (adjustable in Parametric analysis) (Wright, 2013)
Condenser	Heat exchanger	• Pressure (state 12): adjustable for judging criterion • Overall heat transfer coefficient: 250 W/(m^2 K) (Li et al., 2019b)
Pump 1	Pump	• Isentropic efficiency: 60%–95% (adjustable in Parametric analysis) (Wright, 2013) • Vapor fraction (state 15): 0
Pump 2	Pump	• Isentropic efficiency: 60%–95% (adjustable in Parametric analysis) (Wright, 2013)
Pump 3	Pump	• Cooling source temperature: 25 °C • Cooling source Pressure: 101.325 kPa • Mass flow rate of cooling source: 2.0 kg/s • Isentropic efficiency: 60%–95% (adjustable in Parametric analysis) (Wright, 2013)
Pump 4	Pump	• Isentropic efficiency: 60%–95% (adjustable in Parametric analysis) (Wright, 2013) • Output pressure (state 18): 101.325 kPa

used Peng–Robinson equations of state were adopted to solve the thermodynamic properties of each state. The objectives of η_E and W_{exp} are optimized by adopting an optimization procedure, in addition to the basic calculation process are similar to that of our previous studies (Chen et al., 2021). Taking the system complexity and parameter coupling effect into consideration, the maximums of η_E is realized by maximizing the exergy of output for the whole system, and the W_{exp} is maximized for the TPC subsystem. The pressure drop in the flash tank (ΔP_{ft}), flow rate of the cyclic working fluid, and discharge temperature (T_{dis}, temperature of state 6) are assumed and adjusted as optimization variables. The optimal solution is conducted by the optimizer in Aspen Hysys, which is based on the Box algorithm. It is theoretically based on Box's Complex method and is applied to deal with non-linear objective problems (Box, 1965). Fig. 4 presents the optimization procedure of the proposed system. The detailed input parameters are listed in Table 1. Table 2 shows the parameters of the system analysis. ΔT_{cond} and ΔT_{evap} represent the pinch point temperature difference in heat exchangers. W_{exp}^{max} represents the maximum mechanical work that the expander can generate.

The specific operation strategy of the proposed system is as follows. Adjusting the ΔP_{ft} will cause the mass flow of state 2 to move inversely to that of state 5. That is, as the ΔP_{ft} rises, the mass flow of state 2 will increase and the mass flow rate of state 5 will decrease, indicating that the W_{com} will increase whereas the W_{exp}^{max} will decrease. In the TPC subsystem, parameter optimization is conducted for the maximization of the W_{exp} (Fig. 4). From the point of the whole system, the W_{com} is all supplied by the W_{exp}^{max}. If $W_{exp}^{max} > W_{com}$, the ΔP_{ft} should be increased to meet the above requirements. Instead, the ΔP_{ft} needs to be decreased. The optimal ΔP_{ft} is determined by repeated regulation.

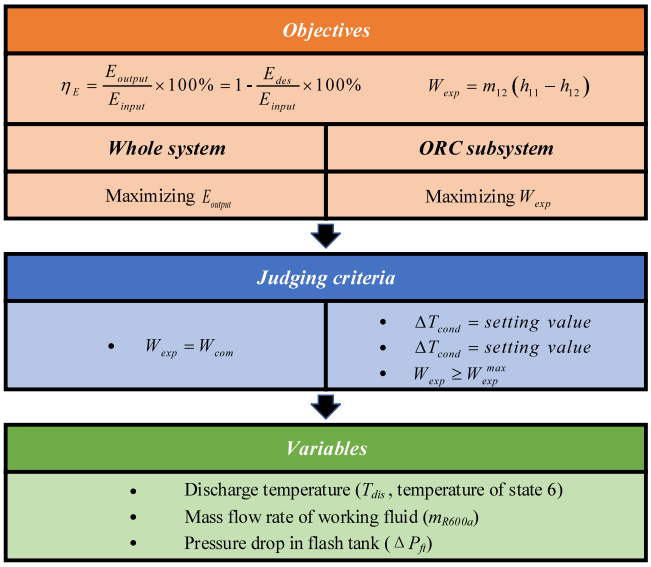

Fig. 4. The optimization procedure of the proposed system.

Table 2
Parameters of system analysis.

Parameter	Value	Parameter	Value
T_0	25 °C	C_{cool}	0.35 $/GJ (Cui et al., 2019)
P_0	101.325 kPa	C_{ele}	8.72 × 10^{-3} $/kWh (Guangdong Provincial Development and Reform Commission, PRC, 2015)
ΔT_{cond}	3 °C (Kemp, 2010)	i	5%
ΔT_{evap}	3 °C (Kemp, 2010)	N	25 years

4. Result and discussion

4.1. Selection of the TPC subsystem and the cyclic working fluid

In this section, to select suitable TPC subsystems, the ORC–based system (i.e., the proposed system with ORC) and T–CO_2–based system (i.e., the proposed system with T–CO_2 cycle) are

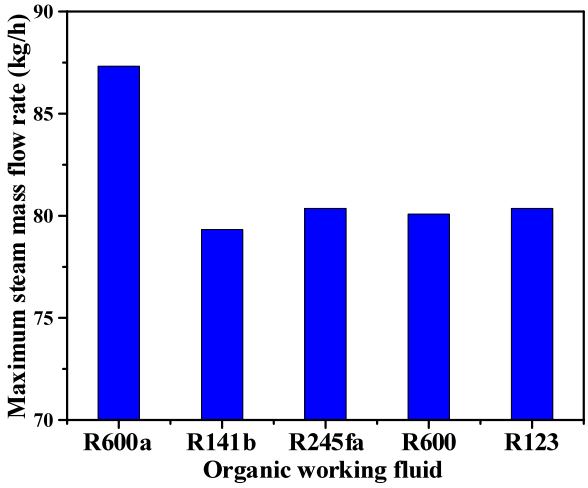

Fig. 5. Maximum steam mass flow rate for different organic refrigerants.

simulated and evaluated through four indicators: the steam mass flow rate, exergy efficiency, total costs, and COS. The selection of proper cyclic working fluid contributes to the minimization of entropy production as well as basically determining the operability and economy of the TPC subsystems. CO_2 is the working media of the T–CO_2 cycle. Compared with the steam Rankine cycle, ORC is more similar to the steam compression refrigeration cycle; hence; that all organic refrigerants can be employed as the working medium of ORC over a certain temperature range. Consequently, the selection of organic refrigerants is an important task. First of all, their impacts on the environment and their safety need to be concerned. That is, a suitable organic refrigerant should be characterized by zero ozone destruction potential (ODP), low global warming potential (GWP), high thermal stability, non-toxic, and non-combustible. In addition to their properties, ORC working mediums also need to meet the requirements for safe and stable operation of the ORC. Dry fluid and isentropic fluid are mostly applied in the ORC, which are saturated vapor at the outlet of the evaporator without overheating. Considering the cost and safety of the system, the ORC working medium with lower critical pressure is a better choice. What is more, its critical temperature should be close to that of the heat source for better temperature matching. Hence, R600a, R141b, R245fa, R600, and R123 are primarily selected for the ORC–based system and the properties are provided in Table 3. For the proposed system, the steam mass flow rate is selected to evaluate the thermodynamic performance when the above five fluids are applied. As revealed by Fig. 5, the system with R600a has the largest steam mass flow rate, which means that the system performs better in thermodynamics. This is because the critical temperature of R600a is close to the heat source temperature. Therefore, R600a is selected as the working fluid of the ORC–based system.

For further study, the comparative analysis among the ORC–based and T–CO_2–based systems is conducted under the same input parameters, which are listed in Table 1. The parameters of each cycle are adjusted to maximize the η_{sp}, and the thermodynamic properties of states are listed in Table S3 in the Supporting Information. The various cost calculations of the T–CO_2–based system and ORC–based system are listed in Table S4 in the Supporting Information.

Fig. 6 presents the comparisons among the thermodynamic and economic performance of the ORC–based system and T–CO_2–based system. As shown in Fig. 6, the thermodynamic and economic performance of the two cycles is quite different. To be specific, the maximum steam mass flow rate of the T–CO_2–based system can reach 187.34 kg/h, which is twice that of the ORC–based. But it is at the expense of the η_E of the T–CO_2–based system. The η_E of the T–CO_2–based system is only 26.15%, which is 69.41% less than that of the ORC–based system. Through further exergy analysis of each component (Fig. 7), it can be found that the E_{des} of the T–CO_2–based system is significantly greater than that of the ORC–based system. The low η_E (26.16%) of the T–CO_2–based system attributes to substantial exergy wasted in the pumps, condenser, flash tank, and expander. This is inevitable for the T–CO_2–based system as the W_{pumps}, W_{exp}, and the heat transfer of the condenser increase with the increase of the steam mass flow. From the economic perspective, there are obvious advantages in the ORC–based system with 56.61% and 9.66% larger annual total costs and COS than the T–CO_2–based system. The component costs of the proposed system with different TPC cycles vary greatly (Fig. 8): the costs of the components (evaporator, compressor, pumps), the costs of maintenance, and electricity are obviously fewer of the ORC–based system compared with the T–CO_2–based system. The tremendous circulation pressure in the T–CO_2–based system causes a noticeable rise in equipment costs and costs of maintenance. The cooling water consumption increases because of a larger heat exchange capacity of the condenser, and the cost of electricity increases due to the huge mechanical work consumption of pumps. The higher steam mass flow rate of the T–CO_2–based system prevents the COS from increasing dramatically, but it is at the cost of consuming a large amount of electricity, which defeats the purpose of the proposed system.

In conclusion, the T–CO_2–based system has obvious advantages in improving the η_{sp}. However, the low η_E and the large COS may become its fatal defect. The η_E of the T–CO_2–based system will increase as the steam mass flow rate decreases, but it also means that the COS of the T–CO_2–based system will increase significantly because of the huge total costs. How to reduce the cost of the T–CO_2–based system is a focus of future research in this field. Accordingly, taking into account the investment costs, the equipment requirements, and the operating conditions, the ORC–based system is more suitable than the T–CO_2–based system in this paper and the ORC–based system is selected as TPC cycle under the condition that the thermodynamic and economic performance are comprehensively considered.

4.2. Parametric analysis

To further investigate the system performance, the effects of some key parameters, such as the flow rate of R600a (m_{R600a}), steam compression ratio, isentropic efficiency of the expander, and the adiabatic efficiency of pumps, are analyzed under different heat source conditions. The W_{exp}, mechanical work input from the grid, η_E, η_{sp}, and COS are chosen to visualize the effects of the parameters in the section.

4.2.1. Effects of the R600a flow rate

In this section, the effect of the m_{R600a} under designed working conditions is studied, in which stats 11 is always in the saturated vapor state (i.e., the fluid flowing into the expander is a saturated gas). As can be seen in Fig. 9a, the W_{exp} curves and the η_E curves corresponding to different heat source temperatures have the same fluctuation trend with an increase in the m_{R600a}. T_{hs} represents the temperature of heat source. Take the heat source of 100 °C as an example, there is a gradual rise of W_{exp} from 0.1 to 0.25 kg/s, then an observable dip. The largest W_{exp} can reach 6.04 kW, which occurs when the m_{R600a} is 0.25 kg/s. Meanwhile, the W_{exp} is positively associated with the heat source temperature. The reasons for this phenomenon are as follows. The W_{exp} is the

Table 3
Properties of common organic refrigerants.

Organic refrigerant	R600a	R141b	R245fa	R600	R123
Normal boiling point/°C	−11.67	32.00	14.90	−0.5	27.82
Critical temperature/°C	134.67	204.40	154.05	151.90	183.68
Critical pressure/MPa	3.60	4.21	3.60	3.79	3.60
ODP	0	0.086	0	0	0.01
GWP/(100 yr)	20	630	820	20	93
Type	Dry fluid	Dry fluid	Dry fluid	Dry fluid	Isentropic fluid

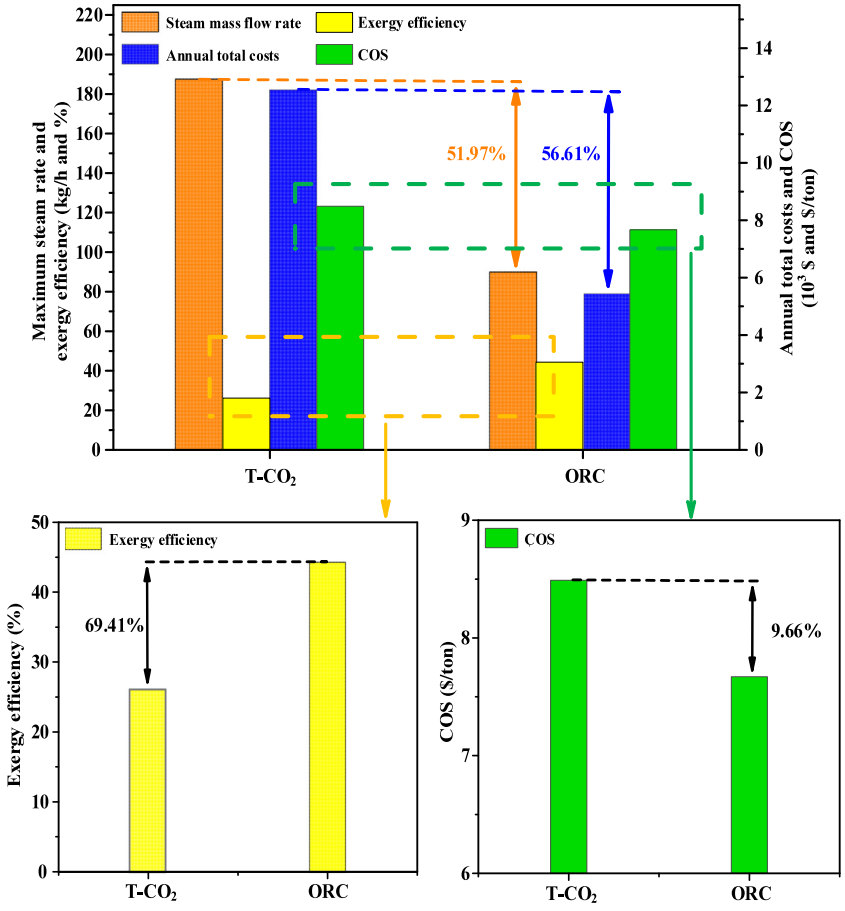

Fig. 6. Thermodynamic and economic performance of the ORC–based system and T–CO_2–based system.

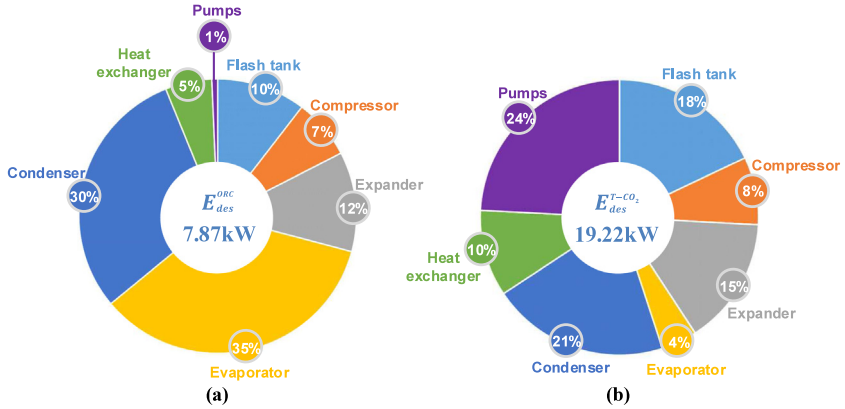

Fig. 7. Ratio of exergy destruction of each equipment for the (a) ORC–based system and (b) T–CO_2–based system.

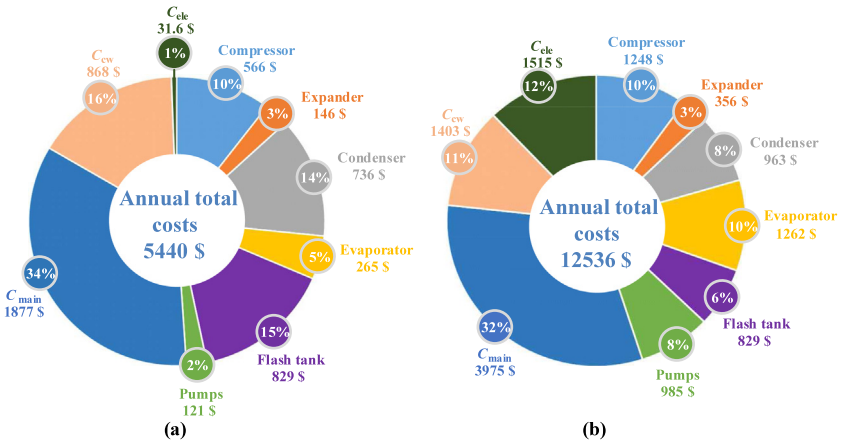

Fig. 8. Ratio of component costs and operation & maintenance expense for the (a) ORC–based system and (b) T–CO_2–based system.

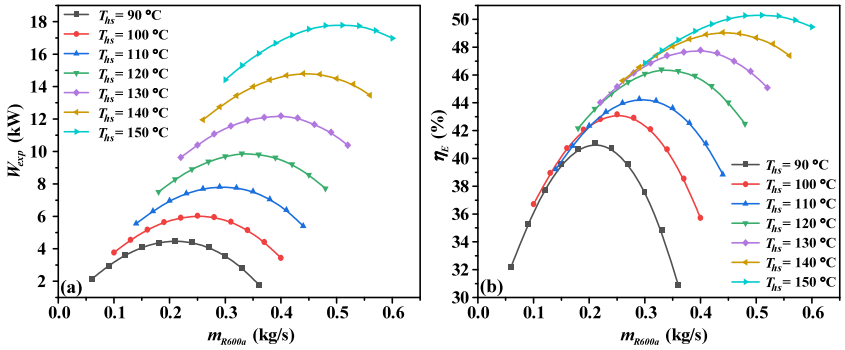

Fig. 9. The effect of m_{R600a} and heat source temperature on the (a) W_{exp} and the (b) η_E.

product of the m_{R600a} and the specific enthalpy difference (Δh). Fig. 10 illustrates the variations of specific enthalpy difference of the expander (Δh_{exp}) and decrement of specific enthalpy difference (Δh^*_{exp}) versus the m_{R600a}. The rise of the m_{R600a} causes a significant dip in Δh_{exp}, whereas the Δh^*_{exp} shows an overall upward trend, which means that the Δh_{exp} is shrinking at an increasing rate. Hence, the m_{R600a} is the dominant factor of W_{exp} in the early stage. As the m_{R600a} exceeds a certain value, the W_{exp} begins to decline because of the rapid drop in enthalpy difference. From another perspective, Fig. 11 presents the visual depiction of the relationship between pinch point location and m_{R600a}, in which the minimum approach temperature of the evaporator is 3 °C constantly. The location where the minimum approach temperature occurs is the pinch point location. Before the peak value of W_{exp}, pinch point moves to the right when the m_{R600a} rises. After the maximum W_{exp}, the pinch point moves left quickly, which means that the temperature of the ORC working fluid at state 11 is lower to meet the requirement of reaching the pinch point earlier. Thus, a continued rise of the m_{R600a} leads to a sharp dip in the temperature difference of the expander, which further causes a rapid decline in W_{exp}. Synthesizing the above analysis, there is a pattern that W_{exp} increased firstly and decreased later.

Fig. 9b visualizes that, as far as the η_E is concerned, the main trend of the η_E is upward and then downward. The specific reasons in the case of the 100 °C heat source are demonstrated in Fig. 12, which provides the effects of m_{R600a} on the E_{input}, E_{output}, and E_{des}. There are obvious turning points of the E_{des}. That is, before reaching the turning point, the E_{des} decreases rapidly. After reaching the turning point, the E_{des} begins to increase gradually. But the E_{input} remains the same, because it only depends on the heat source conditions. According to Eq. (4), there is a sharp rise in η_E, then a steep dip. The same results can be obtained from

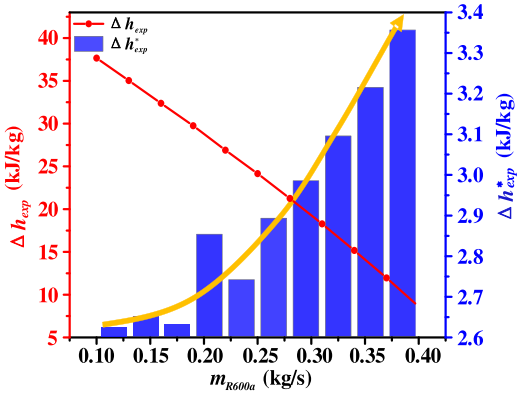

Fig. 10. The variation of the expander specific enthalpy difference and decrement of specific enthalpy difference versus m_{R600a} in the case of 100 °C heat sources.

the point of view of E_{input}. Under other heat source conditions, the analyses of the reason for the changes in the W_{exp} and the η_E is similar to the above, shown in Fig. S1 and Fig. S2 in the Supporting Information.

4.2.2. Effects of the isentropic and adiabatic efficiency of expander and pump

Keeping the m_{R600a} and T_{dis} constant, which are listed in Table 4, visual depictions of the expander isentropic efficiency and pumps adiabatic efficiency effect are present in Figs. 13 and 14. The W_{exp} and the mechanical work input from the grid rise steadily as the isentropic and adiabatic efficiency increase,

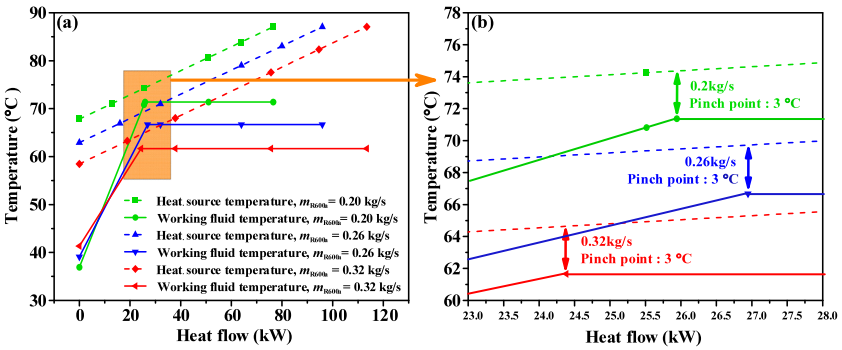

Fig. 11. The variation of the pinch point position versus m_{R600a} in the case of 100 °C heat sources.

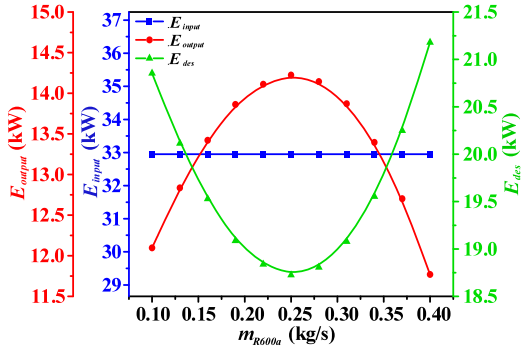

Fig. 12. The variation of the E_{input}, E_{output}, and E_{des} with the simultaneous variation of the m_{R600a} in the case of 100 °C heat sources.

thereby increasing the E_{output} while the E_{input} keeps unchanged. Hence, the rises in the isentropic and adiabatic efficiencies cause a monotonous rise in the η_E. Additionally, when the isentropic efficiency of expander and the adiabatic efficiency of pumps change the same value, the effect of the former on the thermodynamic performance is obviously greater than that of the latter.

4.2.3. Effects of the steam compression ratio

In practical application, the pressure of the required steam will vary according to different requirements. In this section, the effect of the steam compression ratio is performed under a fixed fluid state of state 11 (saturated vapor state), and both the steam (states 4 and 8) and the heat source (state 1) are saturated.

Fig. 15 demonstrates the variations of (a) η_{sp}, (b) η_E, and (c) COS versus steam compression ratio and heat source temperature. The increase in steam compression ratio leads to a great dip in the η_{sp} and then the rate of decline in that slows down, which means that the changes gradually stabilize (Fig. 15a). A similar tendency as above can be observed in analyzing the effect of the steam compression ratio on the η_E in Fig. 15b. Additionally, it is noticeable that an increase in heat source temperature is accompanied by an increase in the η_{sp} and η_E. The reason analyses are as follows. As the steam compression ratio increases (that is, the steam pressure increases and the hot water pressure remains unchanged in this section), the W_{exp} increases accordingly. Under the premise of $W_{exp} = W_{com}$, the mass flow rate of steam must be reduced to reduce the mechanical work consumption of the compressor, as shown in Fig. 16b. Besides, as the steam compression ratio increases, the flow rate of steam decreases, and the mass exergy of steam increases (Fig. 16b). The decline rate of the former is larger than the growth rate of the latter, leading to a decrease in the exergy of steam (Fig. 16a). Meanwhile, the mechanical work consumption of pumps is proportional to the steam compression ratio and the E_{input} remains constant. Combining the above analyses and Eqs. (4)–(6), the η_E decreases with increasing steam compression ratio. From an economic perspective, an opposite tendency as above can be seen in analyzing the effect of the steam compression ratio on the COS in Fig. 15c, that is, the COS appears in a pattern of monotone increasing. It is caused by changes in the steam flow rate and investment costs. On the one hand, increasing the steam compression ratio results in a significant decline in the flow rate of steam. On the other hand, the W_{exp}, W_{com}, W_{pumps}, Q_{evap}, and Q_{cond} all increase with the rise of the steam compression ratio, resulting in the increment of the $C_{capital}$ and the C_{OM}. Combined with the two aspects, it is seen that the COS will increase monotonically based on Eq. (7).

According to the above analyses, lower steam compression ratio and higher heat source temperature are beneficial to improve thermodynamic and economic performance. Nevertheless, the actual situation should be taken into account. From the perspective of heat source temperature, low-temperature heat sources (<90 °C) perform poorly in terms of economy and thermodynamics. The temperature of the wasted hot water is below 151.8 °C generally in China (Chen et al., 2021). For the steam compression

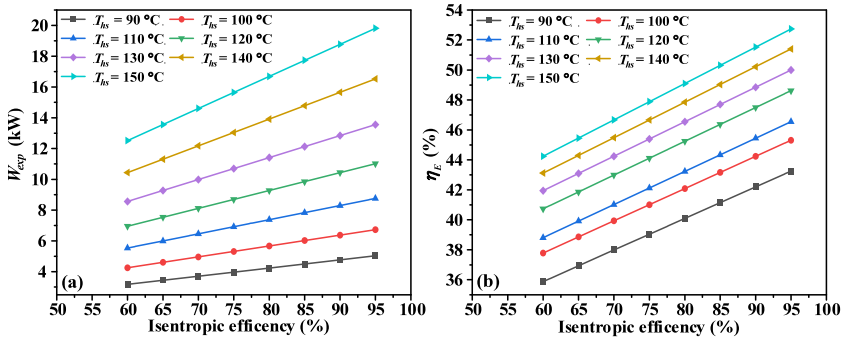

Fig. 13. The effect of the isentropic of expander on the (a) W_{exp} and the (b) η_E.

Table 4
The constant R600a flow rate and discharge temperature.

Heat source temperature/(°C)	90	100	110	120	130	140	150
m_{R600a}/(kg/s)	0.212	0.250	0.314	0.352	0.384	0.442	0.528
T_{dis}/(°C)	60	64	66	70	74	76	76

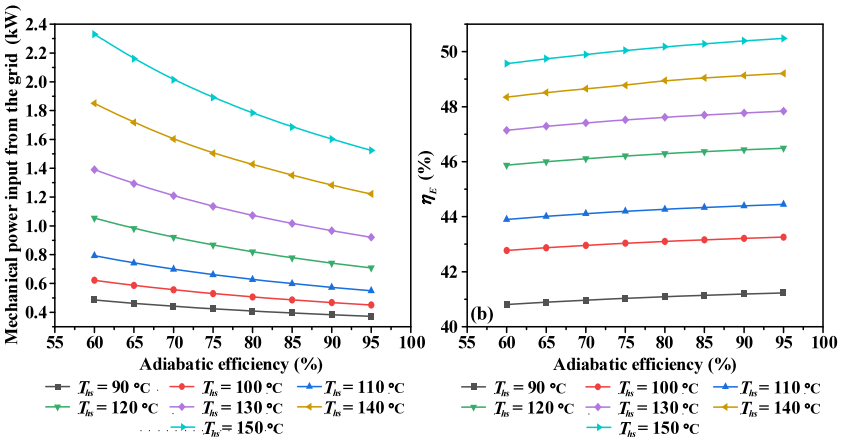

Fig. 14. The effect of the adiabatic efficiency of pumps on the (a) mechanical work input from the grid and (b) η_E.

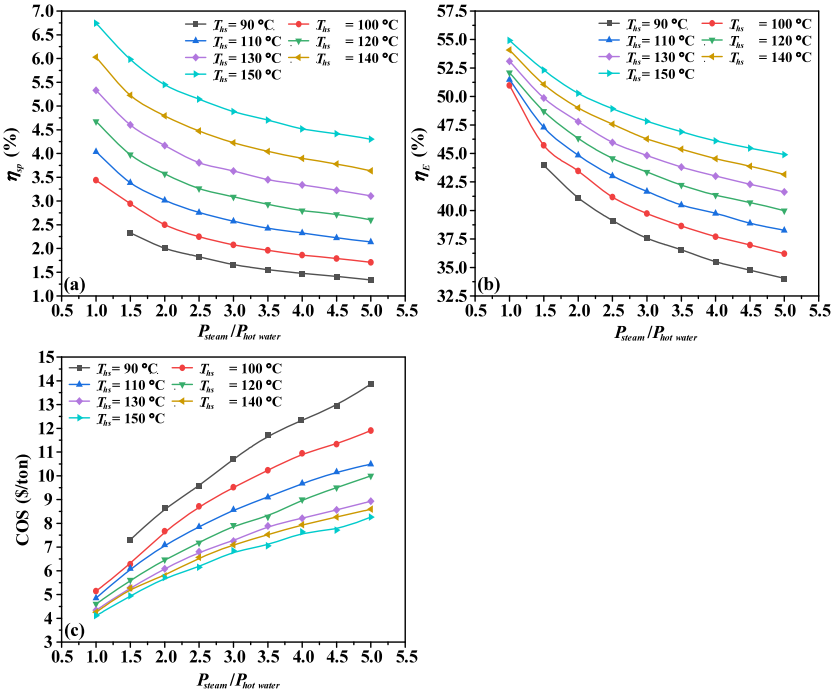

Fig. 15. The effect of the steam compression ratio on the (a) η_{sp}, (b) η_E, and (c) COS.

ratio, it may be necessary to achieve the goal of a high steam compression ratio through multi-stage compression, which is not conducive to simplifying the system. The steam compression ratio should be determined by the actual steam requirements and the heat source conditions. The suitable range of the steam compression ratio is 1–3 under the heat source temperature of 90–150 °C.

4.3. Optimized results

In this section, the parameters are optimized for the purposed of maximizing thermodynamic performance using the optimizer in Aspen Hysys. Under the premise of setting the calculation parameters in Tables 1 and 2, selecting the ΔP_{ft}, T_{dis}, and m_{R600a} as the parameters that need to be optimized. The optimization process was carried out under the heat sources of 90 °C and 100 °C, and the steam compression ratio is 2. Fig. 17 visualizes that under the premise that the W_{exp} can meet the W_{com}, the ΔP_{ft} can reach 24.0 kPa and 38.5 kPa under designed heat source conditions, respectively. Meanwhile, it can be found that the optimal value of the m_{R600a} declines gradually with the T_{dis} rise. As shown by the optimization results (Table 5), for the common case where the heat source temperature is 100 °C, the system η_E is optimal at the m_{R600a} of 0.227 kg/s and the T_{dis} of 63.3 °C. The η_{sp} is 2.50%, and the $\eta_{thermal\ recovery}$ can achieve a relatively high value of 21.34%. From the perspective of exergy, the η_E of the ORC–based system is 44.31%, benefiting from the synthetic

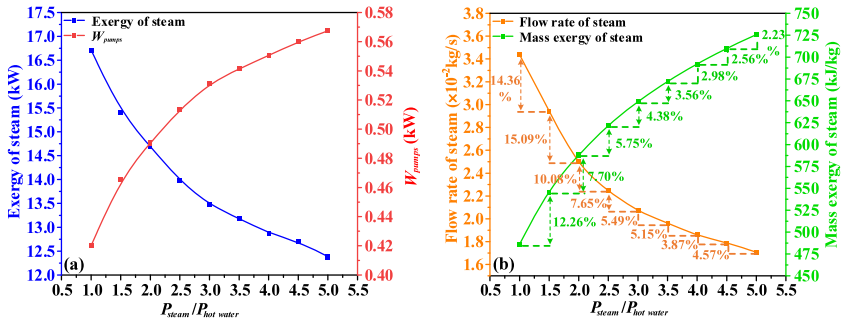

Fig. 16. The variation of (a) the exergy of steam, mechanical work consumption of pumps, (b) flow rate of steam, and mass exergy of steam under the influence of steam compression ratio in the case of 100 °C heat sources.

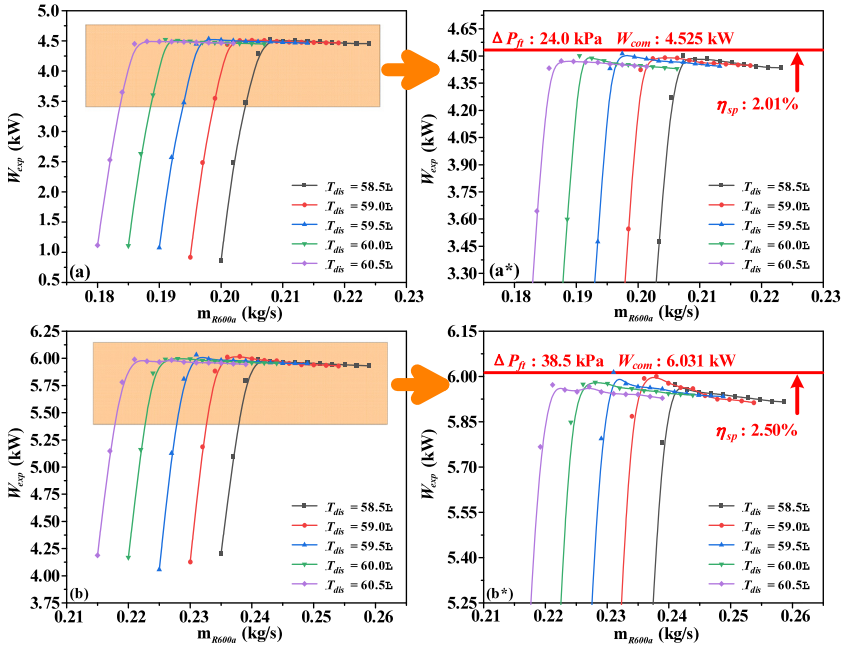

Fig. 17. The combined effect of R600a flow rate and discharge temperature on system performance under heat source temperature of (a) 90 °C and (b) 100 °C.

Table 5
Optimization results.

Temperature of heat source/(°C)	90	100
m_{R600a}/(kg/s)	0.201	0.227
T_{dis}/(°C)	59.4	63.3
ΔP_{ft}/(kPa)	24.0	38.5
η_{sp}/(%)	2.01	2.50
η_E/(%)	41.37	44.31

cascade utilization of energy. What is more, a COS of 7.67 $/ton could be approached in the optimum condition.

5. Conclusions

In this study, a steam generation system, which utilizes low-grade waste heat, is investigated by in-depth thermodynamic and economic analyses. Several investigations have been done on the TPC system, ORC working fluid, control parameter for system optimization. On the basis of models and evaluations in our previous work, thermodynamic and economic screenings of five organic working fluids and two TPC-based systems are conducted to determine the selection of fluid and TPC subsystem. Moreover, the effects of the ORC working fluid flow rate, isentropic and adiabatic efficiency of the expander and pumps, and steam compression ratio on system performance are investigated. The main conclusions are summarized as follows:

(1) Compared with the T-CO_2–based system, the η_E of the ORC–based system is 69.41% higher, while the η_{sp} is 51.97% lower. Meanwhile, the ORC–based system performed better in terms of economics with 56.61% lower annual total cost and 9.66% lower COS. For the background and application scenario of the proposed system, the ORC–based system is a more suitable choice. Moreover, for the selection of ORC working fluid, the ORC–based system with R600a has a higher steam mass flow rate because of a smaller temperature difference between the R600a critical temperature and heat source temperature.

(2) There is an optimum flow rate of ORC working fluid for thermodynamic performance. The mechanical work generation of the expander, mechanical work input from the grid, and η_E increase linearly with the increase of equipment efficiency. Besides, to improve the system performance, the steam compression ratio and the heat source temperature should be reduced and raised respectively within a certain range. Combined with the actual situation, the suitable range of the steam compression ratio is 1–3 under the heat source temperature of 90–150 °C.

(3) Setting the optimum operating parameters, the η_{sp}, η_E, and COS of the ORC–based system are 2.50%, 44.31%, and

7.67 $/ton under the heat source condition of 100 °C. The optimal m_{R600a} decreases gradually with the increase of the T_{dis}.

To sum up, the proposed system provides a technically feasible and cost–competitive solution for waste heat utilization and steam generation in the industry. Facing various working conditions, the simulation results provide theoretical guidance under operations with different configurations and states.

CRediT authorship contribution statement

Zhiyong Zeng: Supervision, Writing (original draft), Visualization, Funding acquisition. **Yufeng Chen:** Conceptualization, Software, Visualization, Writing (original draft). **Chenghao Li:** Software, Visualization, Writing (review & editing). **Yunfeng Li:** Writing (review & editing). **Xiaozan Wu:** Conceptualization, Supervision, Writing (review & editing), Funding acquisition.

Declaration of competing interest

The authors declare that they have no known competing financial interests or personal relationships that could have appeared to influence the work reported in this paper.

Data availability statement

The data used to support the findings of this study are included within the article and supplementary information files.

Acknowledgments

This work was supported by the National Natural Science Foundation of China (Grant No. 52074348) and Fundamental Research Funds for the Central Universities of Central South University (Grant No. 1053320192040).

Appendix A. Supplementary data

Supplementary material related to this article can be found online at https://doi.org/10.1016/j.egyr.2021.08.178.

References

Ammar, Y., Joyce, S., Norman, R., Wang, Y., Roskilly, A.P., 2012. Low grade thermal energy sources and uses from the process industry in the UK. Appl. Energy 89, 3–20. http://dx.doi.org/10.1016/j.apenergy.2011.06.003.

Arpagaus, C., Bless, F., Uhlmann, M., Schiffmann, J., Bertsch, S.S., 2018. High temperature heat pumps: Market overview, state of the art, research status, refrigerants, and application potentials. Energy 152, 985–1010. http://dx.doi.org/10.1016/j.energy.2018.03.166.

Bao, J., Zhang, L., Song, C., Zhang, N., Zhang, X., He, G., 2020. Comparative study of combined organic Rankine cycle and vapor compression cycle for refrigeration: Single fluid or dual fluid? Sustain. Energy Technol. Assess. 37, 100595. http://dx.doi.org/10.1016/j.seta.2019.100595.

Box, M.J., 1965. A new method of constrained optimization and a comparison with other methods. Comput. J. 8, 42–52. http://dx.doi.org/10.1093/comjnl/8.1.42.

Calli, O., Colpan, C.O., Gunerhan, H., 2021. Thermoeconomic analysis of a biomass and solar energy based organic Rankine cycle system under part load behavior. Sustain. Energy Technol. Assess. 46, 101207. http://dx.doi.org/10.1016/j.seta.2021.101207.

Chen, Y., Li, C., Zeng, Z., 2021. Proposal and comprehensive analysis of an innovative steam generation system by deep recovery of low-grade waste heat. J. Clean. Prod. 310, 127509. http://dx.doi.org/10.1016/j.jclepro.2021.127509.

Chen, R., Rao, Z., Liao, S., 2018. Determination of key parameters for sizing the heliostat field and thermal energy storage in solar tower power plants. Energy Convers. Manage. 177, 385–394. http://dx.doi.org/10.1016/j.enconman.2018.09.065.

Cui, P., Yu, M., Liu, Z., Zhu, Z., Yang, S., 2019. Energy, exergy, and economic (3E) analyses and multi-objective optimization of a cascade absorption refrigeration system for low-grade waste heat recovery. Energy Convers. Manage. 184, 249–261. http://dx.doi.org/10.1016/j.enconman.2019.01.047.

El-Sattar, H.A., Kamel, S., Vera, D., Jurado, F., 2020. Tri-generation biomass system based on externally fired gas turbine, organic rankine cycle and absorption chiller. J. Clean. Prod. 260, 121068. http://dx.doi.org/10.1016/j.jclepro.2020.121068.

Fitó, J., Ramousse, J., Hodencq, S., Wurtz, F., 2020. Energy, exergy, economic and exergoeconomic (4E) multicriteria analysis of an industrial waste heat valorization system through district heating. Sustain. Energy Technol. Assess. 42, 13–15. http://dx.doi.org/10.1016/j.seta.2020.100894.

Frate, G.F., Ferrari, L., Desideri, U., 2019. Analysis of suitability ranges of high temperature heat pump working fluids. Appl. Therm. Eng. 150, 628–640. http://dx.doi.org/10.1016/j.applthermaleng.2019.01.034.

Guangdong Provincial Development and Reform Commission, PRC, 2015. The announcement of the price of electricity transmission and distribution areas in our province. http://drc.gd.gov.cn/spjg/content/post_846353.html (accessed 5 June 2021).

Iglesias Garcia, S., Ferreiro Garcia, R., Carbia Carril, J., Iglesias Garcia, D., 2018. A review of thermodynamic cycles used in low temperature recovery systems over the last two years. Renew. Sustain. Energy Rev. 81, 760–767. http://dx.doi.org/10.1016/j.rser.2017.08.049.

Jouhara, H., Khordehgah, N., Almahmoud, S., Delpech, B., Chauhan, A., Tassou, S.A., 2018. Waste heat recovery technologies and applications. Therm. Sci. Eng. Prog. 6, 268–289. http://dx.doi.org/10.1016/j.tsep.2018.04.017.

Kang, D.H., Na, S.I., Yoo, J.W., Lee, J.H., Kim, M.S., 2019. Experimental study on the performance of a steam generation heat pump with the internal heat exchanging effect. Int. J. Refrig. 108, 154–162. http://dx.doi.org/10.1016/j.ijrefrig.2019.09.003.

Kemp, P., 2010. Pinch Analysis and Process Integration, second ed. Butterworth Heinemann, Oxford.

Li, C., Liu, J., Zheng, S., Chen, X., Li, J., Zeng, Z., 2019a. Performance analysis of an improved power generation system utilizing the cold energy of LNG and solar energy. Appl. Therm. Eng. 159, 113937. http://dx.doi.org/10.1016/j.applthermaleng.2019.113937.

Li, C., Zheng, S., Li, J., Zeng, Z., 2019b. Optimal design and thermo-economic analysis of an integrated power generation system in natural gas pressure reduction stations. Energy Convers. Manage. 200, 112079. http://dx.doi.org/10.1016/j.enconman.2019.112079.

Liao, G., Liu, L., E, J., Zhang, F., Chen, J., Deng, Y., Zhu, H., 2019. Effects of technical progress on performance and application of supercritical carbon dioxide power cycle: A review. Energy Convers. Manage. 199, 111986. http://dx.doi.org/10.1016/j.enconman.2019.111986.

Liu, Y., Han, J., You, H., 2020. Exergoeconomic analysis and multi-objective optimization of a CCHP system based on LNG cold energy utilization and flue gas waste heat recovery with CO2 capture. Energy 190, 116201. http://dx.doi.org/10.1016/j.energy.2019.116201.

Lu, Z., Gong, Y., Yao, Y., Luo, C., Ma, W., 2019. Development of a high temperature heat pump system for steam generation using medium-low temperature geothermal water. Energy Procedia 158, 6046–6054. http://dx.doi.org/10.1016/j.egypro.2019.01.513.

Lu, H., Price, L., Zhang, Q., 2016. Capturing the invisible resource: Analysis of waste heat potential in Chinese industry. Appl. Energy 161, 497–511. http://dx.doi.org/10.1016/j.apenergy.2015.10.060.

Mateu-Royo, C., Mota-Babiloni, A., Navarro-Esbrí, J., Peris, B., Molés, F., Amat-Albuixech, M., 2019. Multi-objective optimization of a novel reversible High-Temperature Heat Pump-Organic Rankine Cycle (HTHP-ORC) for industrial low-grade waste heat recovery. Energy Convers. Manage. 197, 111908. http://dx.doi.org/10.1016/j.enconman.2019.111908.

Minea, V., 2014. Power generation with ORC machines using low-grade waste heat or renewable energy. Appl. Therm. Eng. 69, 143–154. http://dx.doi.org/10.1016/j.applthermaleng.2014.04.054.

National Bureau of Statistics, PRC, 2017. China Statistical YearBook. https://data.stats.gov.cn/easyquery.htm?cn=C01 (accessed 5 June 2021).

Parrado, C., Girard, A., Simon, F., Fuentealba, E., 2016. 2050 LCOE (Levelized Cost of Energy) projection for a hybrid PV (photovoltaic)-CSP (concentrated solar power) plant in the Atacama Desert, Chile. Energy 94, 422–430. http://dx.doi.org/10.1016/j.energy.2015.11.015.

Quoilin, S., Broek, M. Van Den, Declaye, S., Dewallef, P., Lemort, V., 2013. Techno-economic survey of Organic Rankine Cycle (ORC) systems. Renew. Sustain. Energy Rev. 22, 168–186. http://dx.doi.org/10.1016/j.rser.2013.01.028.

Saleh, B., Koglbauer, G., Wendland, M., Fischer, J., 2007. Working fluids for low-temperature organic Rankine cycles. Energy 32, 1210–1221. http://dx.doi.org/10.1016/j.energy.2006.07.001.

Sarkar, J., 2015. Review and future trends of supercritical CO2 Rankine cycle for low-grade heat conversion. Renew. Sustain. Energy Rev. 48, 434–451. http://dx.doi.org/10.1016/j.rser.2015.04.039.

Sinasac, Z., Jianu, O.A., 2021. Parametric study on the exergetic and cyclic performance of a solar-powered organic Rankine cycle coupled with a thermal energy storage and complete flashing cycle. Sustain. Energy Technol. Assess. 45, 101172. http://dx.doi.org/10.1016/j.seta.2021.101172.

Sun, Z., Lai, J., Wang, S., Wang, T., 2018. Thermodynamic optimization and comparative study of different ORC configurations utilizing the exergies of LNG and low grade heat of different temperatures. Energy http://dx.doi.org/10.1016/j.energy.2018.01.085.

Wang, Q., Liu, X., Guo, X., 2017. Application of waste heat recovery technology in union station and analysis of energy efficiency. Procedia Eng. 205, 3860–3866. http://dx.doi.org/10.1016/j.proeng.2017.10.063.

Wang, B., Qi, L., Zhang, W., 2019. Technical transformation of recovery and utilization of reaction waste heat in phthalic anhydride production process. Henan Chem. Ind. 4, 75–84. http://dx.doi.org/10.14173/j.cnki.hnhg.2019.02.014, (in Chineses).

Wang, L., Yu, S., Kong, F., Sun, X., Zhou, Y., Zhong, W., Lin, X., 2020a. A study on energy storage characteristics of industrial steam heating system based on dynamic modeling. Energy Rep. 1–9. http://dx.doi.org/10.1016/j.egyr.2020.07.001.

Wang, N., Zhang, S., Fei, Z., Zhang, W., Shao, L., Sardari, F., 2020b. Thermodynamic performance analysis a power and cooling generation system based on geothermal flash, organic Rankine cycles, and ejector refrigeration cycle; application of zeotropic mixtures. Sustain. Energy Technol. Assess. 40, 100749. http://dx.doi.org/10.1016/j.seta.2020.100749.

Wright, T., 2013. Fluid Machinery: Perforamnce, Analysis, and Design. CRC press LLC, Boca Raton.

Xu, J., 2011. Practice and Benefit analysis of waste heat utilization of printing and dyeing wastewater. J. Shaoxing Univ. 31, 73–76. http://dx.doi.org/10.16169/j.issn.1008-293x.k.2011.02.017, (in Chinese).

Yu, H., Feng, X., Wang, Y., 2016. Working fluid selection for organic rankine cycle (ORC) considering the characteristics of waste heat sources. Ind. Eng. Chem. Res. 55, 1309–1321. http://dx.doi.org/10.1021/acs.iecr.5b02277.

Zhang, Y., Zhang, Y., Yu, X., Guo, J., Deng, N., Dong, S., He, Z., Ma, X., 2017. Analysis of a high temperature heat pump using BY-5 as refrigerant. Appl. Therm. Eng. 127, 1461–1468. http://dx.doi.org/10.1016/j.applthermaleng.2017.08.072.

Zhou, N., Wang, X., Chen, Z., Wang, Z., 2013. Experimental study on Organic Rankine Cycle for waste heat recovery from low-temperature flue gas. Energy 55, 216–225. http://dx.doi.org/10.1016/j.energy.2013.03.047.